

Occupation probabilities of valence orbitals relevant to neutrinoless double β decay of ^{124}Sn A. Shrivastava^{1,2,*}, K. Mahata^{1,2}, I. Stefan³, M. Assié³, P. Adsley³, D. Beaumel³, V. M. Datar^{2,4}, A. Georgiadou³, J. Guillot³, F. Hammache³, N. Keeley⁵, Y. H. Kim⁶, A. Meyer³, V. Nanal⁷, V. V. Parkar^{1,2} and N. de Séréville³¹Nuclear Physics Division, Bhabha Atomic Research Centre, Mumbai 400085, India²Homi Bhabha National Institute, Anushaktinagar, Mumbai 400094, India³Université Paris-Saclay, CNRS/IN2P3, IJCLab, 91405 Orsay, France⁴India-based Neutrino Observatory, Tata Institute of Fundamental Research, Mumbai 400005, India⁵National Centre for Nuclear Research, ul. Andrzeja Sołtana 7, 05-400 Otwock, Poland⁶GANIL, CEA/DRF - CNRS/IN2P3, boulevard Henri Becquerel, BP 55027, F-14076 Caen Cedex 5, France⁷Department of Nuclear and Atomic Physics, Tata Institute of Fundamental Research, Mumbai 400005, India

(Received 16 June 2021; revised 30 November 2021; accepted 20 December 2021; published 6 January 2022)

Neutron transfer reaction measurements, relevant to the neutrinoless double β decay candidate ^{124}Sn and its daughter ^{124}Te , have been performed. Precise measurements of both neutron addition [(d, p) , (^4He , ^3He)] and removal [(p, d) , (^3He , ^4He)] cross sections have been used to determine the occupation of valence orbitals pertinent to neutrinoless double β decay in these two nuclei. This information could be used to constrain calculations of the nuclear matrix element for the neutrinoless double β decay of ^{124}Sn . The change in the ground-state neutron vacancies in proceeding from ^{124}Sn to ^{124}Te is mainly found in the $d_{3/2,5/2}$ and $h_{11/2}$ orbitals. The occupancies of states near the Fermi level are in reasonable agreement with shell model calculations.

DOI: [10.1103/PhysRevC.105.014605](https://doi.org/10.1103/PhysRevC.105.014605)

I. INTRODUCTION

The search for the as yet unobserved rare process, neutrinoless double β decay ($0\nu\beta\beta$), is crucial in the quest for physics beyond the standard model [1–4]. Observation of such a process would immediately demonstrate that neutrinos are their own antiparticles (i.e., Majorana fermions) and violation of conservation of lepton number ($\Delta L = 2$). The corresponding decay rate may give the first direct estimate of the absolute neutrino mass scale, provided that the uncertainty in calculations of the nuclear matrix element can be reduced. Major experiments are being performed and planned worldwide on different nuclei that are possible candidates for this decay.

The main obstacle in extracting the neutrino mass from the half-life of this decay is the uncertainty in the calculated nuclear matrix element. While significant progress has been made in the calculation of nuclear matrix elements (NMEs) for $0\nu\beta\beta$ decay, there are still substantial differences in the results using different methods. Hence there is a need to constrain these NMEs through experiments [5]. However, obtaining experimental constraints on these calculations remains a challenge as there is no obvious experimental probe that connects the initial and final ground states in a manner that approximates the transition operator for neutrinoless double β decay [3,5–7].

Direct experimental information on the matrix elements for neutrinoless double β decay is extremely challenging, if not impossible, to obtain. The decay involves virtual intermediate states of very high excitation energies and angular momenta

with a wide range of multipolarities; hence the matrix elements deduced from single or double β decays with real neutrinos cannot be assumed to be appropriate to extract reliable information for the neutrinoless mode. In the absence of any other experimentally accessible process, indirect methods to determine the matrix element can be useful [7]. The wave functions of the initial and final states are one of the main inputs in calculating the nuclear matrix element. The wave functions are calculated based on different nuclear models, including the configuration interaction shell model (ISM) and quasiparticle random phase approximation (QRPA). Single-nucleon transfer reactions can be used to characterize the ground-state wave functions while two neutron transfer reactions can explore BCS-like correlations between zero angular momentum coupled nucleon pairs [7]. Pioneering studies of neutron-addition and -removal reactions on isotopes in the $A = 76$ system, where ^{76}Ge is a candidate for $0\nu\beta\beta$ decay, together with proton-addition reactions, provided information on the energies and vacancies of the valence orbitals of ^{76}Ge and ^{76}Se [8,9]. The results indicated that the Fermi surface is much more diffuse than that used in theoretical calculations. It was shown later that by adjusting the assumed single-particle energies, the matrix element for the ^{76}Ge to ^{76}Se transition was reduced by $\approx 25\%$ compared to the previous QRPA value and consequently the calculated decay rate changed by about a factor of 2 [10–13]. Similar measurements have recently been performed on other $0\nu\beta\beta$ decay candidates, viz. ^{130}Te [14], ^{136}Xe [15], and ^{100}Mo [16]. There are several experiments proposed/running to search for double β decay in ^{100}Mo , viz. SuperNEMO [17], AMoRE [18], and CUPID/LUMINEU [19]. ^{76}Ge is under study by the GERDA collaboration [20]. The ^{136}Xe isotope is the subject of the EXO-200 [21] and

*aradhana@barc.gov.in

KamLAND-Zen experiments [22]. The ^{130}Te isotope is being studied for $0\nu\beta\beta$ decay by the CUORE [23] and SNO+ collaborations [24].

In India, a feasibility study to search for $0\nu\beta\beta$ decay in ^{124}Sn has been initiated [25]. The TINTIN experiment (The INdian TIN detector) will be housed at the upcoming India-based Neutrino Observatory (INO) [26], an underground facility with ≈ 1000 m of rock cover all around. In the case of ^{124}Sn and the daughter ^{124}Te , the information on (d, p) , (p, d) , $(^3\text{He}, ^4\text{He})$, and $(^4\text{He}, ^3\text{He})$ reactions is either very limited or not available. The transfer cross sections have been measured previously but not with the same experimental methods and employing different parameters in the DWBA (distorted wave Born approximation) analyses extracting the spectroscopic factors, resulting in large systematic errors. In some cases, the older experiments could only be used as a guide for identifying l values and to indicate which transitions were strong or weak. In the case of ^{124}Sn , data are available for (d, p) [27–30], (p, d) [30–32], and $(^4\text{He}, ^3\text{He})$ [27] reactions. For ^{124}Te , data are available for (d, p) [33,34], (p, d) [35], and $(^3\text{He}, ^4\text{He})$ [35,36] reactions. The aim of the present measurement is to analyze all the results in a consistent manner to permit the extraction of more accurate occupation numbers with a common experimental approach, thus reducing the systematic error. Using both neutron addition and removal reactions allows the use of the Macfarlane and French sum rules [37]. The method consists of requiring a normalization such that for a given orbital characterized by the total angular momentum j , the sum of the measured occupancy and vacancy on the same target add up to the degeneracy of the orbital, $2j + 1$. This normalization procedure is shown to be useful in understanding the uncertainties in orbital occupancies obtained using transfer reactions [8,9].

The paper is organized as follows. Experimental details and results are discussed in Sec. II. Comparisons between the experimental observations and theoretical calculations are presented in Sec. III, followed by a discussion in Sec. IV. Section V contains a brief summary.

II. EXPERIMENTAL DETAILS

Cross section measurements for the (d, p) , (p, d) , $(^4\text{He}, ^3\text{He})$, and $(^3\text{He}, ^4\text{He})$ reactions on enriched ^{124}Te and ^{124}Sn (both 99.9% enriched) foils were performed using the Enge Split Pole magnetic spectrometer, taking beams from the ALTO facility, Laboratoire de Physique des 2 Infinis Irène Joliot-Curie (IJCLab), France. Both targets, around $200 \mu\text{g}/\text{cm}^2$ thick, were deposited on $20 \mu\text{g}/\text{cm}^2$ CVD carbon backings. These are polycrystalline diamond films synthesized using the energy-assisted chemical vapor deposition (CVD) method. The beam energies were chosen to be a few MeV above the Coulomb barrier where the angular distributions are distinctly forward peaked. The (d, p) measurements were carried out at 15 MeV. For the (p, d) reactions the proton energy was selected to be 22 MeV, to ensure that the outgoing deuterons had approximately the same energy as the incident deuterons in the (d, p) reaction. This allows a similar optical model parametrization to be used in the DWBA for both channels, thus minimizing systematic uncer-

ainties. With the same consideration the beam energies for the $(^4\text{He}, ^3\text{He})$ and $(^3\text{He}, ^4\text{He})$ reactions were selected to be 40 MeV and 30 MeV, respectively. For the $(^4\text{He}, ^3\text{He})$ and $(^3\text{He}, ^4\text{He})$ reactions, the main interest was in the $l = 5$ and $l = 4$ transfers. As the DWBA approximation is usually most accurate at the first maximum of the angular distribution of transfer products, the data were taken at angles corresponding to the first maxima for the relevant l transfers in each reaction. The spectrometer was kept at angles of 7° and 16° for the (d, p) reactions, 7° and 13° for the (p, d) and $(^4\text{He}, ^3\text{He})$ reactions, and 7° and 20° for the $(^3\text{He}, ^4\text{He})$ reactions. To evaluate the background arising from the ^{12}C present in the backing, measurements were made with a ^{12}C target of thickness $40 \mu\text{g}/\text{cm}^2$ at each angle setting for all four reactions. Beam currents were measured using a Faraday cup placed behind the target inside the scattering chamber.

The scattered particles were momentum analyzed after entering the split-pole spectrometer through a rectangular aperture covering a solid angle of 1.64 msr and were focused on the focal-plane detection system [38]. The magnetic rigidity was deduced from a position-sensitive proportional counter by taking the time difference between the two sides of the delay line. This was followed by another proportional counter and finally a plastic scintillator that provided energy-loss information in the gas and the residual energy of the particle, respectively. Particle identification was achieved by a combination of magnetic rigidity and energy-loss characteristics in the proportional counter and the scintillator. Data were collected up to an excitation energy of around 3 MeV.

In order to obtain absolute differential cross sections, an estimate of the product of the target thickness and spectrometer solid angle is required. This was obtained by measuring elastic scattering in the Coulomb regime at a laboratory angle of 16° for each target using a beam of 20 MeV α particles. At this angle, an error of 0.1° will correspond to a deviation of around 2% in the calculated elastic scattering cross section with respect to the Coulomb scattering estimated by the Rutherford formula. The systematic uncertainties were minimized by keeping the spectrometer aperture fixed throughout the experiment, being the same for the elastic-scattering and the transfer-reaction measurements. The same targets were used, and the same settings on the beam-current integrator were used. For each reaction and angle setting, measurements for ^{124}Sn and ^{124}Te targets were performed back to back.

Tin nuclei with a proton closed shell ($Z = 50$) and Te nuclei with only two protons beyond the $Z = 50$ closed shell span the wide neutron number region $N = 50$ –82. The relevant active orbitals are $0g_{7/2}$, $1d_{3/2,5/2}$, $2s_{1/2}$, and the unique parity $0h_{11/2}$. These states can be populated through $l = 4, 2, 0$, and 5 transfer, respectively. Representative spectra showing the states populated via (p, d) and $(^3\text{He}, ^4\text{He})$ reactions for ^{124}Te are shown in Fig. 1 while those populated via (d, p) and $(^4\text{He}, ^3\text{He})$ reactions on the ^{124}Sn target are shown in Fig. 2. Contaminants arising due to carbon and oxygen present in the target could be identified from magnetic rigidity and did not interfere significantly in the region of interest due to kinematical conditions. The data taken separately with ^{12}C are also plotted to assess contamination due to the carbon backing of the targets. Typical energy resolutions, in terms

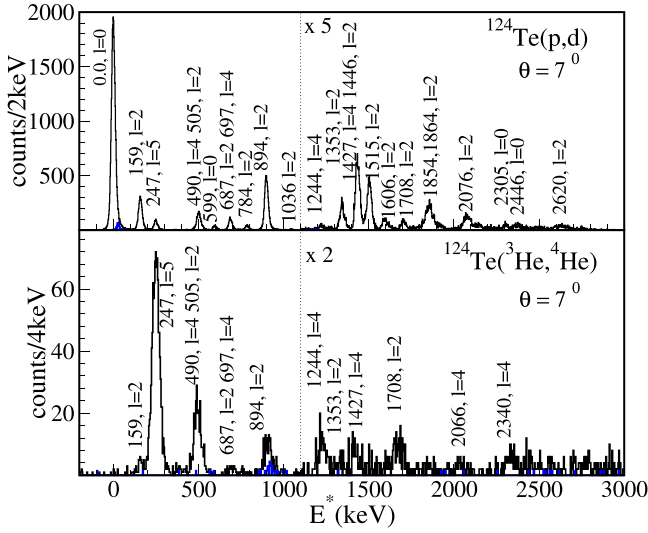


FIG. 1. Excitation energy spectra for the $^{124}\text{Te}(p,d)$ (upper panel) and $^{124}\text{Te}(^3\text{He}, ^4\text{He})$ (lower panel) reactions at 7° . The states corresponding to $\ell = 0, 2, 4$, and 5 of ^{123}Te are labeled. The histogram in blue corresponds to a ^{12}C target.

of full width at half maximum, were around 60 keV for the ($^3\text{He}, ^4\text{He}$), ($^4\text{He}, ^3\text{He}$), and 20 keV for the (p, d), (d, p) reactions. The preferential population of higher angular momentum states with the He isotopes, compared to those with p and d projectiles, can be seen. The $l = 0$ levels are clearly visible in the (p, d) and (d, p) reactions, while they are much weaker in the ($^3\text{He}, ^4\text{He}$) and ($^4\text{He}, ^3\text{He}$) reactions, due to kinematic matching conditions.

III. DWBA ANALYSIS

The Sn and Te nuclei are nearly spherical in shape with predominantly vibrational structures and relatively weak col-

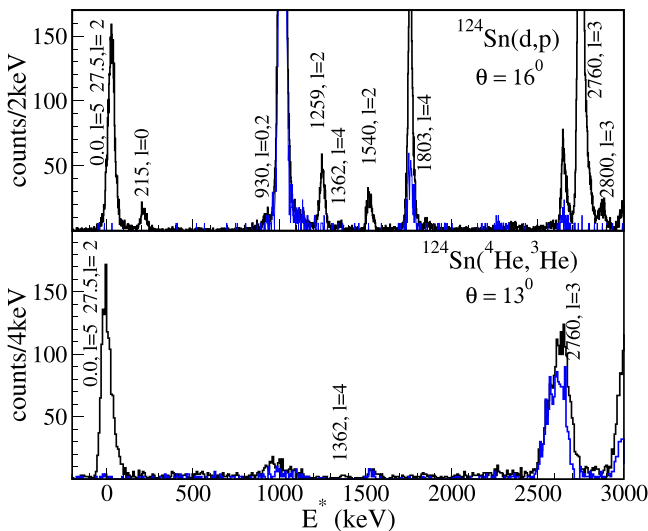


FIG. 2. Excitation energy spectra for the $^{124}\text{Sn}(d,p)$ (upper panel) and $^{124}\text{Sn}(^4\text{He}, ^3\text{He})$ (lower panel) reactions at 16° and 13° , respectively. The states corresponding to $\ell = 0, 2, 4$, and 5 of ^{125}Sn are labeled. The histogram in blue corresponds to a ^{12}C target.

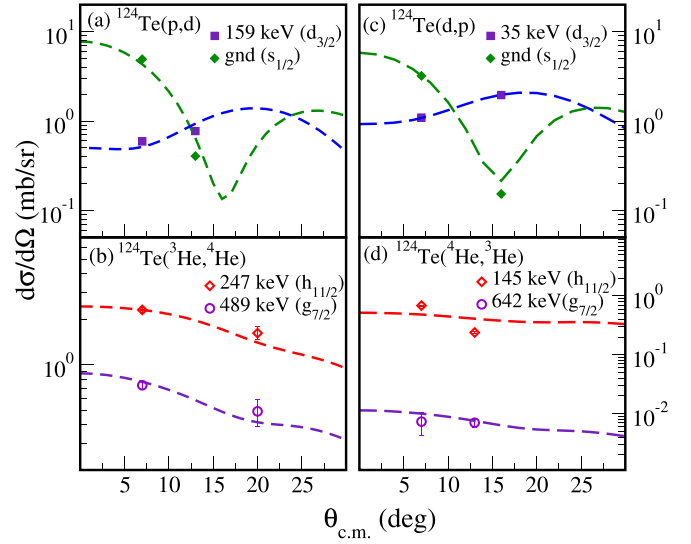


FIG. 3. Transfer cross sections for (a) the first $\ell = 0, 2$ states of ^{123}Te , (b) $\ell = 4, 5$ states of ^{123}Te , (c) $\ell = 0, 2$ states of ^{125}Te , and (d) $\ell = 4, 5$ states of ^{125}Te populated via (p, d), ($^3\text{He}, ^4\text{He}$), (d, p), and ($^4\text{He}, ^3\text{He}$) reactions, respectively. The spectroscopic factors are extracted by scaling the DWBA calculations to best fit the data and are shown as dashed lines.

lective strengths. One would expect the effect of coupled channels to be relatively less important in these cases compared to targets with large deformations (e.g., from the rare-earth region). Hence first-order DWBA calculations can be used to calculate transfer cross sections. In this work, finite-range DWBA calculations were performed using the code FRESKO [39].

For the (d, p) and (p, d) reactions, the proton and deuteron optical potentials were taken from Strömich *et al.* [28]. These potentials are more appropriate to our case than true global ones since they are based on elastic scattering data for targets in the Sn region. Furthermore, recent calculations for the $^{124}\text{Sn}(d, p)$ reaction [29] performed using the optical potentials of Ref. [28] yielded a good description of the cross section and polarization angular distribution data. The Reid soft core binding potential [40] was used to calculate the $d : (p + n)$ overlap.

For the ($^4\text{He}, ^3\text{He}$) and ($^3\text{He}, ^4\text{He}$) reactions the ^4He and ^3He optical potentials were calculated using the global parameters of Avrigeanu *et al.* [41] and Pang *et al.* [42], respectively. The $n + ^3\text{He}$ binding potential was taken from Ref. [43] and is based on *ab initio* calculations.

Spectroscopic factors were obtained by comparing the DWBA calculations to the experimental cross sections. The calculations, normalized to the measured (d, p), (p, d), ($^4\text{He}, ^3\text{He}$), and ($^3\text{He}, ^4\text{He}$) cross sections, are shown in Fig. 3 for ^{124}Te and Fig. 4 for ^{124}Sn . The statistical error on the measured cross section was around 1% to 5% for dominant states and 10% to 15% for weaker states. The target nonuniformity was estimated to be about 5%. The systematic uncertainties on the absolute cross sections arise mainly due to uncertainties in the angle of the spectrometer and the implementation of the Faraday cup and beam current integrator. These are together

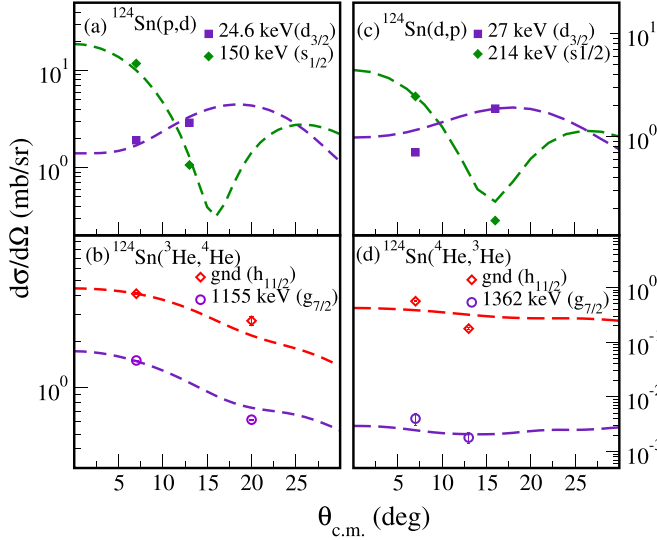


FIG. 4. Transfer cross sections for (a) the first $\ell = 0, 2$ states of ^{124}Sn , (b) $\ell = 4, 5$ states of ^{123}Sn , (c) $\ell = 0, 2$ states of ^{125}Sn , and (d) $\ell = 4, 5$ states of ^{125}Sn populated via (p, d) , $(^3\text{He}, ^4\text{He})$, (d, p) , and $(^4\text{He}, ^3\text{He})$ reactions, respectively. The spectroscopic factors are extracted by scaling the DWBA calculations to best fit the data and are shown as dashed lines.

estimated to be $\approx 3\%$. As can be seen from Fig. 1, in the (p, d) and $(^3\text{He}, ^4\text{He})$ reactions due to kinematic conditions the peaks due to carbon did not interfere in the region of interest. In the case of the (d, p) and $(^4\text{He}, ^3\text{He})$ reactions, the main peaks of interest did not have contamination and for very weakly populated states, at least data from one of the two angles did not have contamination. In the case of contamination from carbon backing, its contributions were subtracted using the carbon target data after scaling for target thickness and beam current, which adds an additional uncertainty of 15%. Detailed data on cross sections along with spectroscopic factors are available as Supplemental Material [44].

Absolute spectroscopic factors obtained this way are sensitive to reaction-model parameters, particularly the bound-state radii and diffuseness. The relative strengths have smaller uncertainty. It has been shown that consistent results can be obtained using the Macfarlane-French sum rule [8]. The method consists of requiring a normalization such that, for a given orbital characterized by total angular momentum j , the sum of the measured occupancy and vacancy on the same target add up to the degeneracy of the orbital, $(2j + 1)$:

$$N_j = [\Sigma(2j + 1)C^2S_{\text{stripping}} + \Sigma C^2S_{\text{pickup}}]/(2j + 1).$$

This normalization procedure helps to understand the uncertainties in using transfer reactions to obtain occupancies and the normalizations obtained are similar to those expected on the basis of the quenching of low-lying single-particle strength observed in $(e, e'p)$ experiments [7]. This procedure was used in the present analysis for states populated in the residual nuclei after transfer reactions on both ^{124}Sn and ^{124}Te . States included were those that had previously known assignments, around 90% of the total strength. The unassigned

strengths not included in the sums to extract the normalization contribute to the uncertainty. For the $s_{1/2}$, $d_{3/2}$, and $d_{5/2}$ states, the spectroscopic factors from the (d, p) neutron addition and (p, d) neutron removal reactions were used to calculate the normalization, N_j , as discussed in [8,9]. Weighted averages were taken of the normalization values deduced from the two targets (^{124}Sn and ^{124}Te). The normalization factors thus obtained for the $2s_{1/2}$ and $1d$ orbitals ($d_{3/2}$ and $d_{5/2}$) were 0.54 (6) and 0.59 (3), respectively. For the high- j states, spectroscopic factors from the $(^4\text{He}, ^3\text{He})$ and $(^3\text{He}, ^4\text{He})$ reactions were used to obtain the normalizations. The extracted normalizations for the $g_{7/2}$ and $h_{11/2}$ levels were found to be 0.63 (27) and 0.65 (6), respectively. In the case of $g_{7/2}$, uncertainty due to the missing strength of around 40% has been added with the availability of results from a recent work [45], that shows the $g_{7/2}$ is not being fully observed in the removal reaction for ^{124}Sn . The normalization values obtained are consistent with those for nearby systems [46].

The neutron vacancies for both ^{124}Sn and ^{124}Te are given in Table I together with recent shell model calculations [47]. Experimental values for neutron vacancies in $^{128,130}\text{Te}$ taken from the literature [46] are also listed in the table. The uncertainties in the vacancies for the $s_{1/2}$ and d states have been estimated based on the values obtained with different sets of optical model potentials [28,48–50] used in the literature [29,30] to analyze the $^{124}\text{Sn}(d, p)$ reaction over a wide angular range at nearby energies and also using potentials from [51–53]. For the $h_{11/2}$ and $g_{7/2}$ states, combinations of potential parameters from Refs. [41,42,54,55] have been used in order to estimate the errors. Figure 5 shows the effect on the DWBA calculations for the $^{124}\text{Sn}(d, p)$ reaction of using a few different combinations of optical model potentials. Uncertainties due to different sets of optical model potentials are less than 10% for each orbital, from the rms deviation on the summed strengths. Uncertainties from unassigned or misassigned strength for weaker transition have been estimated to be of the order of 10%. For $l = 4$, we have added the missing strength of 40% in the uncertainty to account for $g_{7/2}$ not being fully observed in the removal reaction in ^{124}Sn [45]. The error due to statistics was also added in quadrature.

For ^{124}Sn , the change in neutron vacancy with respect to ^{124}Te is shown in Fig. 6 together with the results of calculations using the shell model prescription. As can be seen from Fig. 6(a) and the difference in vacancies plotted in Fig. 6(b), the calculated values for $g_{7/2}$ are overpredicted by the theoretical model for both nuclei. The uncertainty in the difference between the ground-state vacancies in ^{124}Sn and ^{124}Te , plotted in Fig. 6(b), is mainly due to the statistics, as the systematic errors arising due to the same experimental setup and similar optical model parametrization for the DWBA analysis cancel out.

IV. DISCUSSION

The results of the present experiment are compared with those obtained from other candidates for neutrinoless double β decay. It can be seen from Table I that the vacancies in the $\ell = 0, 2$, and 4 states increase in moving from $^{130,128}\text{Te}$ [46] to ^{124}Te , as expected. It should be mentioned that recently a work

TABLE I. Experimentally estimated neutron vacancies in ^{124}Sn and ^{124}Te , together with values from the literature for $^{128,130}\text{Te}$ [46]. The sources of uncertainties are discussed in the text. The results of shell model calculations are also listed [47].

Nucleus	$2s_{1/2}$		$1d_{3/2}$		$1d_{5/2}$		$1d$		$0g_{7/2}$		$0h_{11/2}$		Total	Expected
	Expt.	Calc.	Expt.	Expt.	Expt.	Calc.	Expt.	Calc.	Expt.	Calc.	Expt.	Calc.		
^{124}Sn	0.67(0.19)	0.61	1.67(0.32)	0.53(0.19)	2.23(0.37)	2.08	0.34(0.15)	0.58	4.84(0.74)	4.74	8.08(0.86)		8	
^{124}Te	0.92(0.21)	0.97	2.20(0.29)	1.23(0.30)	3.43(0.42)	2.81	0.43(0.19)	1.00	5.38(0.61)	5.21	10.16(0.79)		10	
^{128}Te	0.72					2.06		0.0		3.34			6.13(0.41)	6
^{130}Te	0.50					1.45		0.0		2.21			4.16(0.41)	4

on $^{112-124}\text{Sn}$ has appeared [45] that provides very similar information specifically on ^{124}Sn using the same technique and shows a close agreement with the present result on neutron vacancies.

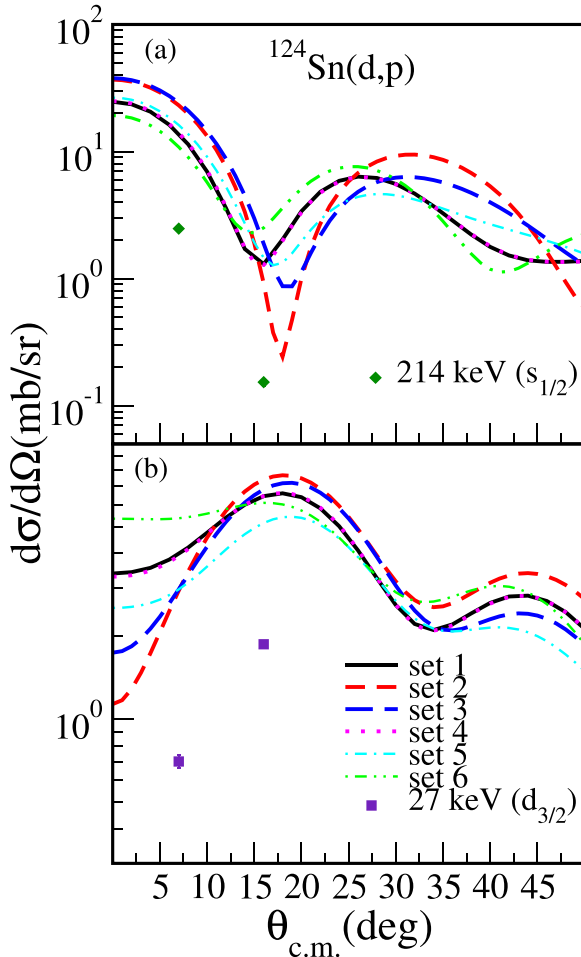


FIG. 5. DWBA calculations using different sets of optical model potential parameters [28,48–53] (with spectroscopic factor $C^2S = 1$) for (d, p) reactions populating the first (a) $\ell = 0$ and (b) $\ell = 2$ states of ^{125}Sn . The different sets of potentials are plotted as solid line for set 1 [28], dashed line for set 2 [48,50], long-dashed line for set 3 [48,49], dotted line for set 4 [28,48], dash-dotted line for set 5 [48,52], and dash-double-dotted line for set 6 [51,53]. Set 1 is that used in Fig. 4(c) to obtain the spectroscopic factor.

For the case of ^{130}Te decaying to ^{130}Xe [14] the most notable feature was the dominance of the $1d$ orbital in the experimentally observed difference between the vacancies of ^{130}Te and ^{130}Xe compared to the theoretical calculations. Furthermore it was found that the $0g_{7/2}$ orbital plays no role, whereas it does in the calculations. Unlike $^{130,128}\text{Te}$, where $\ell = 4$ does not participate in the decay, in the present case of $^{124}\text{Sn} \rightarrow ^{124}\text{Te}$, a small contribution is observed from this state. For ^{136}Xe and ^{100}Mo the experimental neutron occupancies also show disagreement with the theoretical calculations. In the present case of near closed shell nuclei, the model predictions are reasonably good. Measurements on proton occupancies can provide complementary information for studying the favored configuration of neutron pairs decaying into proton pairs. The experimental changes in proton occupancies between the parent and the daughter in the cases of $^{130}\text{Te} \rightarrow ^{130}\text{Xe}$ and $^{136}\text{Xe} \rightarrow ^{136}\text{Ba}$ are found to be similar

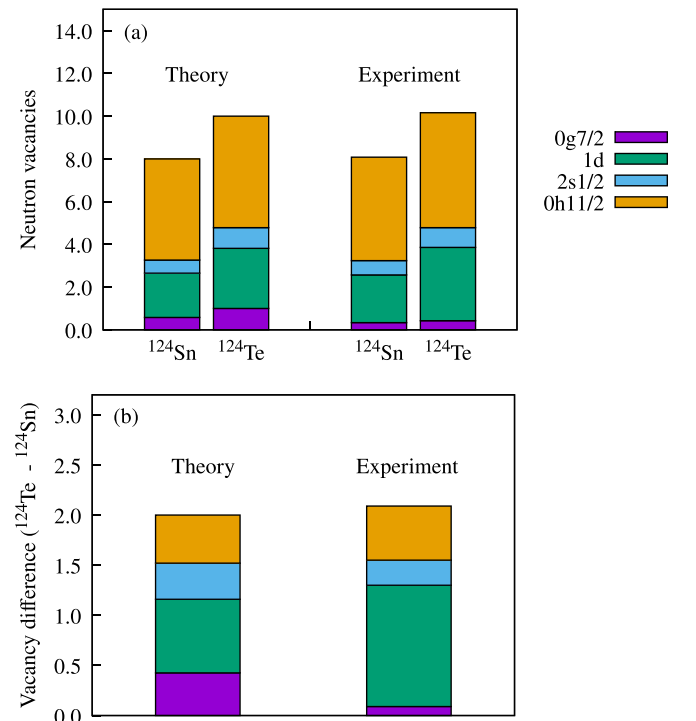


FIG. 6. (a) Experimentally determined neutron vacancies of active orbitals in ^{124}Sn and ^{124}Te plotted together with the calculations reported in Ref. [47] and (b) the difference between the ground-state vacancies in ^{124}Sn and ^{124}Te from both theory and experiment.

[15]. The change is observed mainly in the $0g_{7/2}$ and $1d$ orbitals, where $1d$ is presumed to be mostly the $1d_{5/2}$. It will be very interesting to perform such measurements for both ^{124}Sn and ^{124}Te targets, using the same experimental setup and consistent DWBA analysis, to check whether in this case also the change occurs in $0g_{7/2}$ and $1d_{5/2}$.

V. CONCLUSION

In summary, single-neutron pickup and stripping cross sections have been measured to study the valence neutron composition of the ^{124}Sn and ^{124}Te ground states, providing inputs for constraining calculations of the nuclear matrix element for the neutrinoless double β decay of ^{124}Sn . It is found that the change in the ground-state neutron vacancies for the $^{124}\text{Sn} \rightarrow ^{124}\text{Te}$ transition is mainly in the d and $h_{11/2}$ orbitals, while the $s_{1/2}$ and $g_{7/2}$ orbitals make smaller contributions.

The existing shell model calculations for the present case give similar results for the participation of the valence orbitals. The present measurements are likely to become a significant component of the interpretation of the data, via matrix elements calculated using different theoretical approaches, once the results from the ongoing efforts from the experiment (TINTIN) to measure the neutrinoless double β decay of ^{124}Sn become available.

ACKNOWLEDGMENTS

We thank the ALTO accelerator staff for providing steady and uninterrupted beam and partial support from the French-Indian LIA agreement. We also thank Shri Rohan D. Turbhekar for making targets. V.N. acknowledges the support of the Department of Atomic Energy, Government of India, under Project No. 12-R&D-TFR-5.02-0400.

-
- [1] J. N. Bahcall, H. Murayama, and C. Peña-Garay, *Phys. Rev. D* **70**, 033012 (2004).
- [2] F. T. Avignone, S. R. Elliott, and J. Engel, *Rev. Mod. Phys.* **80**, 481 (2008).
- [3] J. D. Vergados, H. Ejiri, and F. Šimkovic, *Rep. Prog. Phys.* **75**, 106301 (2012).
- [4] Michelle J. Dolinski, Alan W. P. Poon, and Werner Rode-Johann, *Annu. Rev. Nucl. Part. Sci.* **69**, 219 (2019).
- [5] J. M. Yao, L. S. Song, K. Hagino, P. Ring, and J. Meng, *Phys. Rev. C* **91**, 024316 (2015).
- [6] P. K. Rath, R. Chandra, K. Chaturvedi, P. Lohani, P. K. Raina, and J. G. Hirsch, *Phys. Rev. C* **88**, 064322 (2013).
- [7] S. J. Freeman and J. P. Schiffer, *J. Phys. G: Nucl. Part. Phys.* **39**, 124004 (2012).
- [8] J. P. Schiffer, S. J. Freeman, J. A. Clark, C. Deibel, C. R. Fitzpatrick, S. Gros, A. Heinz, D. Hirata, C. L. Jiang, B. P. Kay, A. Parikh, P. D. Parker, K. E. Rehm, A. C. C. Villari, V. Werner, and C. Wrede, *Phys. Rev. Lett.* **100**, 112501 (2008).
- [9] B. P. Kay, J. P. Schiffer, S. J. Freeman, T. Adachi, J. A. Clark, C. M. Deibel, H. Fujita, Y. Fujita, P. Grabmayr, K. Hatanaka, D. Ishikawa, H. Matsubara, Y. Meada, H. Okamura, K. E. Rehm, Y. Sakemi, Y. Shimizu, H. Shimoda, K. Suda, Y. Tameshige *et al.* *Phys. Rev. C* **79**, 021301(R) (2009).
- [10] Fedor Šimkovic, Amand Faessler, and Petr Vogel, *Phys. Rev. C* **79**, 015502 (2009).
- [11] Fedor Šimkovic, Amand Faessler, Herbert Mütter, Vadim Rodin, and Markus Stauff, *Phys. Rev. C* **79**, 055501 (2009).
- [12] J. Suhonen and O. Civitarese, *Phys. Lett. B* **668**, 277 (2008).
- [13] J. Menéndez, A. Poves, E. Caurier, and F. Nowacki, *Phys. Rev. C* **80**, 048501 (2009).
- [14] T. Bloxham, B. P. Kay, J. P. Schiffer, J. A. Clark, C. M. Deibel, S. J. Freeman, S. J. Freedman, A. M. Howard, S. A. McAllister, P. D. Parker, D. K. Sharp, and J. S. Thomas, *Phys. Rev. C* **82**, 027308 (2010).
- [15] S. V. Szewc, B. P. Kay, T. E. Cocolios, J. P. Entwisle, S. J. Freeman, L. P. Gaffney, V. Guimarães, F. Hammache, P. P. McKee, E. Parr, C. Portail, J. P. Schiffer, N. de Séréville, D. K. Sharp, J. F. Smith, and I. Stefan, *Phys. Rev. C* **94**, 054314 (2016).
- [16] S. J. Freeman, D. K. Sharp, S. A. McAllister, B. P. Kay, C. M. Deibel, T. Faestermann, R. Hertenberger, A. J. Mitchell, J. P. Schiffer, S. V. Szewc, J. S. Thomas, and H.-F. Wirth, *Phys. Rev. C* **96**, 054325 (2017).
- [17] R. Arnold *et al.* (NEMO-3 Collaboration), *Phys. Rev. D* **89**, 111101 (2014); **92**, 072011 (2015).
- [18] H. Bhang *et al.*, *J. Phys.: Conf. Ser.* **375**, 042023 (2012).
- [19] A. S. Barabash, D. M. Chernyak, F. A. Danevich, A. Giuliani, I. M. Ivanov, E. P. Makarov, M. Mancuso, S. Marnieros, S. G. Nasonov, C. Nones, E. Olivieri, G. Pessina, D. V. Poda, V. N. Shlegel, M. Tenconi, V. I. Tretyak, Ya. V. Vasiliev, M. Velazquez, and V. N. Zhdankov, *Eur. Phys. J. C* **74**, 3133 (2014).
- [20] M. Agostini *et al.* (GERDA Collaboration), *Phys. Rev. Lett.* **111**, 122503 (2013).
- [21] G. Anton *et al.* (EXO-200), *Phys. Rev. Lett.* **123**, 161802 (2019).
- [22] A. Gando, Y. Gando, T. Hachiya, A. Hayashi, S. Hayashida, H. Ikeda, K. Inoue, K. Ishidoshiro, Y. Karino, M. Koga, S. Matsuda, T. Mitsui, K. Nakamura, S. Obara, T. Oura, H. Ozaki, I. Shimizu, Y. Shirahata, J. Shirai, A. Suzuki, T. Takai, K. Tamae, Y. Teraoka, K. Ueshima, H. Watanabe, A. Kozlov, Y. Takemoto, S. Yoshida, K. Fushimi, T. I. Banks, B. E. Berger, B. K. Fujikawa, T. O'Donnell, L. A. Winslow, Y. Efremenko, H. J. Karwowski, D. M. Markoff, W. Tornow, J. A. Detwiler, S. Enomoto, and M. P. Decowski (KamLAND-Zen Collaboration), *Phys. Rev. Lett.* **117**, 082503 (2016).
- [23] D. R. Artusa *et al.* (CUORE Collaboration), *Adv. High Energy Phys.* **2015**, 879871 (2015).
- [24] Josephine Paton (SNO+ Collaboration), *arXiv:1904.01418*.
- [25] V. Nanal, *EPJ Web Conf.* **66**, 08005 (2014).
- [26] N. K. Mondal, *Pramana* **79**, 1003 (2012).
- [27] C. R. Bingham and D. L. Hillis, *Phys. Rev. C* **8**, 729 (1973).
- [28] A. Strömich, B. Steinmetz, R. Bangert, B. Gonsior, M. Roth, and P. von Brentano, *Phys. Rev. C* **16**, 2193 (1977).
- [29] I. Tomandl, J. Honzátko, T. von Egidy, H.-F. Wirth, T. Faestermann, V. Yu. Ponomarev, S. Pašić, R. Hertenberger, Y. Eisermann, and G. Graw, *Phys. Rev. C* **83**, 044326 (2011).
- [30] L. Gan, H. B. Sun, Z. H. Li, S. P. Hu, Y. J. Li, J. Su, B. Guo, S. Q. Yan, Y. B. Wang, S. Zeng, Z. Y. Han, X. Y. Li, D. H. Li,

- T. L. Ma, Y. P. Shen, Y. Su, E. T. Li, and W. P. Liu, *Phys. Rev. C* **101**, 014612 (2020).
- [31] P. E. Cavanagh, C. F. Coleman, A. G. Hardacre, G. A. Gard, and J. F. Turner, *Nucl. Phys. A* **141**, 97 (1970).
- [32] D. G. Fleming, *Can. J. Phys.* **60**, 428 (1982).
- [33] A. Graue, J. R. Lien, S. Røyrvik, O. J. Aarøy, and W. H. Moore, *Nucl. Phys. A* **136**, 513 (1969).
- [34] J. Honzatko, I. Tomandl, V. Bondarenko, D. Bucurescu, T. von Egidy, J. Ott, W. Schauer, H.-F. Wirth, C. Doll, A. Gollwitzer, G. Graw, R. Hertenberger, and B. D. Valnion, *Nucl. Phys. A* **645**, 331 (1999).
- [35] S. Galés, G. M. Crawley, D. Weber, and B. Zwieglinski, *Nucl. Phys. A* **381**, 173 (1982).
- [36] M. A. G. Fernandes and M. N. Rao, *J. Phys. G: Nucl. Phys.* **3**, 1397 (1977).
- [37] M. H. Macfarlane and J. B. French, *Rev. Mod. Phys.* **32**, 567 (1960).
- [38] R. G. Markham and R. G. Robertson, *Nucl. Instrum. Methods* **129**, 131 (1975).
- [39] I. J. Thompson, *Comput. Phys. Rep.* **7**, 167 (1988).
- [40] R. V. Reid Jr., *Ann. Phys. (NY)* **50**, 411 (1968).
- [41] M. Avrigeanu, W. von Oertzen, A. J. M. Plompen, and V. Avrigeanu, *Nucl. Phys. A* **723**, 104 (2003).
- [42] D. Y. Pang, P. Roussel-Chomaz, H. Savajols, R. L. Varner, and R. Wolski, *Phys. Rev. C* **79**, 024615 (2009).
- [43] I. Brida, Steven C. Pieper, and R. B. Wiringa, *Phys. Rev. C* **84**, 024319 (2011).
- [44] See Supplemental Material at <http://link.aps.org/supplemental/10.1103/PhysRevC.105.014605> for cross sections and spectroscopic factors.
- [45] S. V. Szwec, D. K. Sharp, B. P. Kay, S. J. Freeman, J. P. Schiffer, P. Adsley, C. Binnersley, N. de Séréville, T. Faestermann, R. F. Garcia Ruiz, F. Hammache, R. Hertenberger, A. Meyer, C. Portail, I. Stefan, A. Vernon, S. Wilkins, and H.-F. Wirth, *Phys. Rev. C* **104**, 054308 (2021).
- [46] B. P. Kay, T. Bloxham, S. A. McAllister, J. A. Clark, C. M. Deibel, S. J. Freedman, S. J. Freeman, K. Han, A. M. Howard, A. J. Mitchell, P. D. Parker, J. P. Schiffer, D. K. Sharp, and J. S. Thomas, *Phys. Rev. C* **87**, 011302(R) (2013).
- [47] Mihai Horoi and Andrei Neacsu, *Phys. Rev. C* **93**, 024308 (2016); C. F. Jiao, M. Horoi, and A. Neacsu, *ibid.* **98**, 064324 (2018).
- [48] J. M. Lohr and W. Haerberli, *Nucl. Phys. A* **232**, 381 (1974).
- [49] R. L. Varner, W. J. Thompson, T. L. McAbee, E. J. Ludwig, and T. B. Clegg, *Phys. Rep.* **201**, 57 (1991).
- [50] F. G. Perey, *Phys. Rev.* **131**, 745 (1963).
- [51] A. Koning and J. Delaroche, *Nucl. Phys. A* **713**, 231 (2003).
- [52] F. D. Becchetti Jr. and G. W. Greenlees, *Phys. Rev.* **182**, 1190 (1969).
- [53] Haixia An and Chonghai Cai, *Phys. Rev. C* **73**, 054605 (2006).
- [54] Lynne McFadden and G. R. Satchler, *Nucl. Phys.* **84**, 177 (1966).
- [55] F. D. Becchetti Jr. and G. W. Greenlees, Annual report, J. H. Williams Laboratory, University of Minnesota, 1969.